JOURNAL OF MECHANICS OF MATERIALS AND STRUCTURES
Vol. 4, No. 9, 2009

MODELING DISLOCATION SOURCES AND SIZE EFFECTS AT INITIAL YIELD IN CONTINUUM PLASTICITY

SAURABH PURI, ANISH ROY, AMIT ACHARYA AND DENNIS DIMIDUK

Size effects at initial yield (prior to stage II) of idealized micron-sized specimens are modeled within a continuum model of plasticity. Two different aspects are considered: specification of a density of dislocation sources that represent the emission of dislocation dipoles, and the presence of an initial, spatially inhomogeneous excess dislocation content. Discreteness of the source distribution appears to lead to a stochastic response in stress-strain curves, with the stochasticity diminishing as the number of sources increases. Variability in stress-strain response due to variations of source distribution is also shown. These size effects at initial yield are inferred to be due to physical length scales in dislocation mobility and the discrete description of sources that induce internal-stress-related effects, and not due to length-scale effects in the mean-field strain-hardening response (as represented through a constitutive equation).

1. Introduction

There is a considerable body of experimental evidence that demonstrates that plastic deformation in FCC and other crystalline solids is size dependent at length scales of the order of tens of microns and smaller [Fleck et al. 1994; Ma and Clarke 1995; Stölken and Evans 1998]. Research has suggested that this behavior can be either an effect of constraint imposed on dislocation motion from grain boundaries or internal interfaces or an effect of excess dislocation density resulting from similar externally imposed constraints. However, recently, experiments performed on unconstrained single crystals demonstrated strong size effects at initial yield (including a hardening phenomenon at small strains) as well [Uchic et al. 2004; Dimiduk et al. 2005; Greer et al. 2005; Frick et al. 2008]. This observed phenomenon was modeled within a two-dimensional discrete dislocation (DD) framework [Benzerga et al. 2005; Deshpande et al. 2005; Balint et al. 2006; Benzerga and Shaver 2006] and, more recently using three-dimensional DD techniques [Rao et al. 2008; Tang et al. 2008]. While those studies showed via selected DD frameworks that size effects may arise from aspects of dislocation source properties and source availability, they did not consider that related size effects may arise simply from the dislocation source attributes and heterogeneous spatial arrangement coupling to the boundary constraints when considered completely within a continuum theory for the flow kinematics.

In this paper we examine the question of how dislocation sources may be modeled in continuum plasticity and if the nature of sources contributes to size effects within a continuum representation of idealized simulation cells. We find the answer to be affirmative and use the strategy to demonstrate size effects at initial yield within the context of a recently proposed continuum theory; namely, phenomenological mesoscopic field dislocation mechanics (PMFDM) [Acharya and Roy 2006]. Results obtained from a

Keywords: continuum plasticity, dislocations, finite elements.

finite-element implementation of the theory reasonably accounted for plasticity at mesoscopic scales. Physical length scales exist in the theory and size-affected strain hardening has been demonstrated successfully [Roy and Acharya 2006]. In this paper we specifically discuss size effects at initial yield based on two continuum-level mechanisms. First, size effects are demonstrated in idealized simulation cells having a predefined pattern of statistical dislocation (SD) sources. For the second mechanism, simulations are performed on cells having an initial, spatially inhomogeneous excess dislocation (ED) distribution. Note that the present study is not intended to provide a direct quantitative rationalization of the widely reported experimental findings. Any such attempt would require more advanced quantitative treatments of selected constitutive assumptions, as well as further advances to the computation framework.

In Section 2, a brief description of the governing equations of PMFDM is presented. Section 3 involves discussion of modeling strategy and results so obtained. The paper ends with some concluding remarks in Section 4.

A note regarding terminology: henceforth, given a scale of resolution, l, we refer to the spatial average of Nye's dislocation-density tensor [Nye 1953] over a volume l^3 around a point as the excess dislocation (ED) density tensor at that point. Nye's tensor being a tensorial quantity, the dislocations that on average make no contribution to the net density of Burgers vectors in this process, due to cancellation in sign, form a density that we refer to as the statistically distributed dislocation (SD) density. Thus, the difference of local value of Nye's tensor field and its spatial average (ED) is referred to as SD.

2. Theory

The phenomenological mesoscopic field dislocation mechanics (PMFDM) theory [Acharya and Roy 2006] results from an elementary space-time averaging of the equations of field dislocation mechanics [Acharya 2001; 2003; 2004]. It admits constitutive hypotheses on elasticity, the mean (that is, the space-time average) of signed velocity of dislocation segments (that may be associated with the velocity of mean ED), and the mean slip rate produced by SD. The phenomenology introduced in the model beyond conventional plasticity is meager, with the qualitative predictions of the model not depending upon the phenomenological assumptions. The essential equations of PMFDM are summarized below[1].

The (symmetric) stress tensor $\boldsymbol{T}$ satisfies

$$\boldsymbol{T} = \boldsymbol{C} : \boldsymbol{U}^e, \qquad \operatorname{div} \boldsymbol{T} = \boldsymbol{0}, \tag{1}$$

along with standard traction/displacement boundary conditions. $\boldsymbol{C}$ is the possibly anisotropic fourth order tensor of linear elastic moduli and $\boldsymbol{U}^e$ is the elastic distortion tensor defined as

$$\boldsymbol{U}^e = \operatorname{grad} \boldsymbol{u} - \boldsymbol{U}^p. \tag{2}$$

In this equation, $\boldsymbol{u}$ is the total displacement field and $\boldsymbol{U}^p$ is the plastic distortion tensor which is decomposed uniquely into compatible and incompatible parts as

$$\boldsymbol{U}^p = \operatorname{grad} \boldsymbol{z} - \boldsymbol{\chi}. \tag{3}$$

[1]For motivation behind the formulation the reader is referred to the work of Acharya and Roy [2006].

Thus, the elastic distortion tensor may be rewritten as,

$$\boldsymbol{U}^e = \operatorname{grad}(\boldsymbol{u} - \boldsymbol{z}) + \chi, \tag{4}$$

where the field χ cannot be written as a nontrivial gradient. The incompatible part, χ, is given by

$$\operatorname{curl} \chi = \boldsymbol{\alpha}, \qquad \operatorname{div} \chi = \boldsymbol{0}, \qquad \chi \boldsymbol{n} = \boldsymbol{0} \text{ on } \partial B, \tag{5}$$

where $\boldsymbol{\alpha}$ is the space-time averaged excess dislocation density tensor field and $\boldsymbol{n}$ is the unit normal on the boundary ∂B of the body. The vector field $\boldsymbol{z}$ whose gradient represents the compatible part of $\boldsymbol{U}^p$ obeys the relation

$$\operatorname{div}(\operatorname{grad} \dot{\boldsymbol{z}}) = \operatorname{div}(\boldsymbol{\alpha} \times \boldsymbol{V} + \boldsymbol{L}^p), \qquad (\operatorname{grad} \dot{\boldsymbol{z}})\boldsymbol{n} = (\boldsymbol{\alpha} \times \boldsymbol{V} + \boldsymbol{L}^p)\boldsymbol{n} \text{ on } \partial B, \tag{6}$$

where $\boldsymbol{V}$ and $\boldsymbol{L}^p$ need to be specified constitutively. $\boldsymbol{V}$ represents the velocity of the ED and $\boldsymbol{L}^p$ represents that part of the total slip strain rate which is not represented by the slipping produced by the averaged signed dislocation density (ED). The value of $\dot{\boldsymbol{z}}$ is prescribed at an arbitrarily chosen point of the body and in our case is assumed to vanish without loss of generality. Finally the temporal evolution of the ED density tensor field is prescribed as

$$\dot{\boldsymbol{\alpha}} = -\operatorname{curl} \boldsymbol{S}, \tag{7}$$

where $\boldsymbol{S}$ is the averaged slipping distortion (slip rate) defined as

$$\boldsymbol{S} := \boldsymbol{\alpha} \times \boldsymbol{V} + \boldsymbol{L}^p. \tag{8}$$

2.1. ***Boundary condition on surface flow.*** Equation (7) admits boundary conditions on the dislocation flow [Acharya and Roy 2006]. In general, a natural boundary condition of the form $\boldsymbol{S} \times \boldsymbol{n} = \boldsymbol{\Phi}$, where $\boldsymbol{\Phi}$ is a (second-order tensor valued) specified function of time and position along the boundary satisfying the constraint $\boldsymbol{\Phi n} = \boldsymbol{0}$, is appropriate to model controlled flow at the boundary. A rigid boundary with respect to slipping may be represented with a zero flow boundary condition $\boldsymbol{S} \times \boldsymbol{n} = \boldsymbol{0}$ on the entire boundary. Imposing such a boundary condition can lead to the development of shocks or discontinuities. A less restrictive boundary condition is the imposition of the dislocation flux, $\boldsymbol{\alpha}(\boldsymbol{V} \cdot \boldsymbol{n})$, on inflow points of the boundary (where $\boldsymbol{V} \cdot \boldsymbol{n} < 0$), along with a specification of $\boldsymbol{L}^p \times \boldsymbol{n}$ on the entire boundary. This condition allows free exit of dislocations without any added specification.

2.2. ***Constitutive specification.*** Constitutive specifications for the dislocation-velocity vector, $\boldsymbol{V}$, and the slip-distortion rate due to SDs, $\boldsymbol{L}^p$, are required. Simple choices motivated by conventional plasticity and the thermodynamics of PMFDM (ibid.) are

$$\boldsymbol{L}^p = \dot{\gamma}\, \frac{\boldsymbol{T}'}{|\boldsymbol{T}'|}, \quad \dot{\gamma} \geq 0, \qquad \boldsymbol{V} = v \frac{\boldsymbol{d}}{|\boldsymbol{d}|}, \quad v \geq 0, \tag{9}$$

where $\boldsymbol{T}'$ is the stress deviator, $\dot{\gamma}$ and v are nonnegative functions of state representing the magnitudes of the SD slipping rate and the averaged ED velocity, respectively. The direction of the dislocation velocity is defined by

$$\begin{aligned} &\boldsymbol{d} := \boldsymbol{b} - \Big(\boldsymbol{b} \cdot \frac{\boldsymbol{a}}{|\boldsymbol{a}|}\Big)\frac{\boldsymbol{a}}{|\boldsymbol{a}|}, && \boldsymbol{b} := \boldsymbol{X}(\boldsymbol{T}'\boldsymbol{\alpha}), && b_i = e_{ijk} T'_{jr} \alpha_{rk}, \\ &&& \boldsymbol{a} := \boldsymbol{X}\big(\operatorname{tr}(\boldsymbol{T})\boldsymbol{\alpha}\big), && a_i = \big(\tfrac{1}{3} T_{mm}\big) e_{ijk} \alpha_{jk}. \end{aligned} \tag{10}$$

Thermodynamics indicates $\boldsymbol{b}$ as the driving force for $\boldsymbol{V}$; the definition of $\boldsymbol{d}$ is to ensure pressure independence of plastic straining in the model. We choose a power law relation for $\dot{\gamma}$ as

$$\dot{\gamma} = \dot{\gamma}_0 \left(\frac{|\boldsymbol{T}'|}{\sqrt{2}g} \right)^{1/m}, \tag{11}$$

where m is the rate sensitivity of the material, g is the strength of the material, and $\dot{\gamma}_0$ is a reference strain rate. The expression for υ is assumed to be

$$\upsilon(\text{state}) = \eta^2 b \left(\frac{\mu}{g} \right)^2 \dot{\gamma}\,(\boldsymbol{T}', g), \tag{12}$$

where μ is the shear modulus, b the Burgers vector magnitude and $\eta = 1/3$ a material parameter.

The strength of the material is assumed to evolve according to

$$\dot{g} = \left[\frac{\eta^2 \mu^2 b}{2(g - g_0)} k_0 |\boldsymbol{\alpha}| + \theta_0 \left(\frac{g_s - g}{g_s - g_0} \right) \right] \{ |\boldsymbol{\alpha} \times \boldsymbol{V}| + \dot{\gamma} \}, \tag{13}$$

where g_s is the saturation stress, g_0 is the yield stress, and θ_0 is the stage II hardening rate. The material parameters g_s, g_0, μ, b, $\dot{\gamma}_0$, and m are known from conventional plasticity (Voce law and power-law hardening). Consequently, k_0 is the only extra parameter that needs to be fitted and can be obtained from experimental grain-size dependence of flow stress results, as shown in [Acharya and Beaudoin 2000; Beaudoin et al. 2000].

The finite-element discretization for the system of equations above is discussed in [Roy and Acharya 2006]. Here we only summarize the finite-element discretization of (7), which has an extra term in the weak formulation corresponding to the least-squares finite-element discretization of the inflow boundary condition on $\boldsymbol{\alpha}$ [Varadhan et al. 2006].

In the following expression, the symbol $\delta(\,\cdot\,)$ represents a variation (or test function) associated with the field $(\,\cdot\,)$ in a suitable class of functions. An increment of time $[t, t+\Delta t]$ is considered, and fields without any superscripts refer to values at $t + \Delta t$ and those with the superscript t refer to values at time t. All spatial fields are discretized by first-order, 8-node (three-dimensional), isoparametric brick elements. A mixed forward-backward Euler scheme is adopted as

$$\begin{aligned}
&\int_B \delta\alpha_{ij}(\alpha_{ij} - \alpha_{ij}^t)\,d\upsilon - \Delta t \int_B [\delta\alpha_{ij,k}\alpha_{ij}v_k^t - \delta\alpha_{ij,k}\alpha_{ik}v_j^t]\,d\upsilon - \Delta t \int_B \delta\alpha_{ij}s_{ij}^t\,d\upsilon + \Delta t \int_{\partial B_i} \delta\alpha_{ij}F_{ij}\,da \\
&\quad + \Delta t \int_{\partial B_o} \delta\alpha_{ij}\alpha_{ij}^t(v_k^t n_k)\,da - \Delta t \int_{\partial B} \delta\alpha_{ij}\alpha_{ik}^t n_k v_j^t\,da - \Delta t \int_B \delta\alpha_{ij,k}e_{jkl}L_{il}^p\,d\upsilon \\
&\quad + \Delta t \int_{\partial B} \delta\alpha_{ij}e_{jkl}L_{il}^p n_k\,da + \int_{B_{\text{interiors}}} A_{ri}(\delta\alpha_{ri} + \Delta t[\delta\alpha_{ri,j}v_j^t + \delta\alpha_{ri}v_{j,j}^t - \delta\alpha_{rj,j}v_i^t - \delta\alpha_{rj}v_{i,j}^t])\,d\upsilon \\
&\qquad\qquad + \Delta t \int_{\partial B_i} \delta\alpha_{ij}\big(F_{ij} - \alpha_{ij}^t(v_k^t n_k)\big)\,da = 0,
\end{aligned} \tag{14}$$

where

$$A_{ri} = \alpha_{ri} - \alpha_{ri}^t + \Delta t[\alpha_{ri,j}^t v_j^t + \alpha_{ri}^t v_{j,j}^t - \alpha_{rj,j}^t v_i^t - \alpha_{rj}^t v_{i,j}^t - s_{ri}^t + e_{ijk}L_{rk,j}^p]. \tag{15}$$

$\boldsymbol{F}$ is the prescribed flux on the inflow boundary (∂B_i), ∂B_o is the set of outflow/neutral points of the boundary where $\boldsymbol{V} \cdot \boldsymbol{n} \geq 0$, and $B_{\text{interiors}}$ refers to the union of the element interiors. $\delta\alpha_{ij}$ is arbitrary up to

satisfying any prescribed essential boundary conditions. The term on the last line of (14) is an additional term that enters the discretization for excess dislocation density evolution for all the computations in this paper over those described in [Roy and Acharya 2006]. The scheme is consistent even without the addition of this term; numerical experiments show a better imposition of inflow boundary conditions with its inclusion.

3. Results and discussion

Unless otherwise mentioned, material parameters used for all the computational experiments are

$$b = 4.05 \times 10^{-4}\,\mu\text{m}, \quad m = 1.0, \quad g_s = 161\,\text{MPa}, \quad g_0 = 17.3\,\text{MPa}, \quad \theta_0 = 392.5\,\text{MPa}, \quad k_0 = 20.0.$$

The reference strain rate is $\dot{\gamma}_0 = 1\,\text{sec}^{-1}$. Isotropic elastic constants of the representative material, aluminum, are $E = 62.78\,\text{GPa}$, $\nu = 0.3647$, where E is the Young's modulus and ν is the Poisson's ratio.

A comment on the rate sensitivity value is in order. Our intent here is to model a situation where dislocations move in unobstructed, free-flight mode in large parts of the body. Under these circumstances, and with the understanding that rate insensitivity is a manifestation of very fast motions homogenized in time with near stationary events, it is only reasonable to utilize a rate sensitivity parameter value representative of linear drag in our simulations.

The initial conditions corresponding to the field equations mentioned in Section 2 are as follows. For the $\boldsymbol{u}$ field we assume $\boldsymbol{u}|_{t=0} \equiv \boldsymbol{0}$, which is a physically natural initial condition on the displacement field. Unless otherwise mentioned, we assume that the body is initially ED-free which translates to $\boldsymbol{\alpha}|_{t=0} \equiv \boldsymbol{0}$. The initial condition on the grad z field is obtained from solving (1) and (5) with $\boldsymbol{u}|_{t=0} \equiv \boldsymbol{0}$ and the value of z set to zero at a single arbitrary point in the body.

Time-dependent simple-shearing solutions are studied numerically. The imposed boundary conditions corresponding to such a loading are as follows: displacements on the bottom face are constrained in all three directions while those on the top, left and right faces are constrained in the x_2 and x_3 directions only (see Figure 1). The front and back faces are displacement-constrained in the x_3 direction and traction free in the x_1 and x_2 directions. The displacements corresponding to a simple shear strain are prescribed

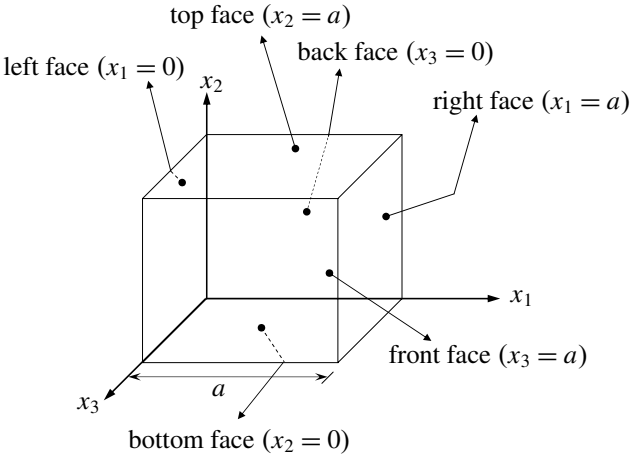

Figure 1. Schematic layout of a typical model geometry.

through the kinematic boundary condition

$$u_1(x_1, x_2, x_3, t) = d(x_2)\dot{\Gamma}t \tag{16}$$

on the nodes of the left, right, top, and bottom faces. Here, $d(x_2)$ is the height, from the bottom of the cube, of the point with coordinates (x_1, x_2, x_3). Γ is the average engineering shear strain given by the ratio of the applied horizontal displacement of the top surface to the cube height, $\dot{\Gamma}$ is an applied shear strain rate of 1 sec^{-1}, and t is time.

All computations are performed on one of two desktop machines with 2 GB and 8 GB RAM, respectively. In the interpretation of results, the symbol τ refers to the nominal (reaction) shear traction on the top surface of the simulation cell.

3.1. ***Dislocation source distribution.*** The effect of physical dimensions of the simulation cell (having a predefined distribution of SD sources) on the initial yield strength is described in this section. First we discuss how a Frank–Read source is grossly represented in our framework. In general, a Frank–Read source produces dislocation loops that cannot be sensed if their size is less than the scale of resolution. However, once the loop expands up to the scale of resolution, it can be sensed as demonstrated in Figure 2a. In order to numerically simulate (SD) dislocation sources in the framework of PMFDM, the size of the region representing a source is assumed to be greater than or equal to the scale of resolution (see Figure 2b). In the interior of the source region there are no EDs due to cancellation in signs during

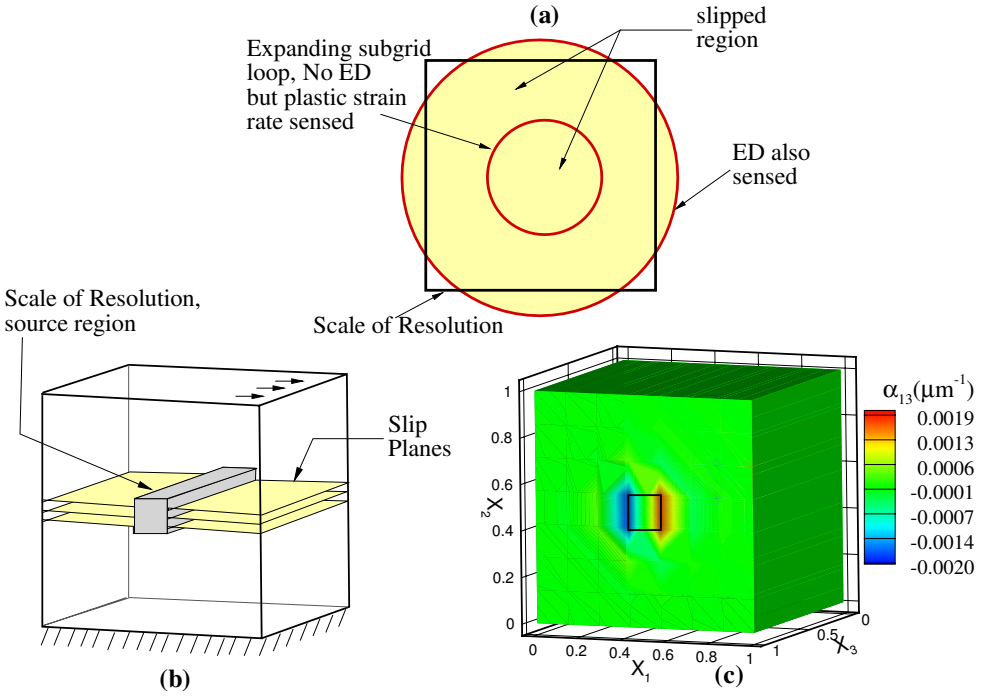

Figure 2. Top: physical representation of a Frank–Read source. Bottom left: representation of a numerically simulated Frank–Read Source. Bottom right: excess dislocation density at $\Gamma = 0.1\%$ for pattern (a).

averaging. This corresponds to the physical situation of the dislocation loop not being sensed when its size is smaller than the scale of resolution. The plastic strain rate corresponding to the motion of these unresolved dislocations, however, is sensed, and is taken into account through $\boldsymbol{L}^p$. At the interface between the slipped and unslipped regions, EDs are observed due to the gradient in plastic strain rate (7) and (8). This observation corresponds to the physical definition of a dislocation loop being sensed when its size equals or exceeds the scale of resolution. A simple test is performed to demonstrate this idea. Consider a cubical cell of edge length of 1.0 μm and discretized into a finite element grid. The element at the center is the dislocation source region, as shown in Figure 2b. The cell is unstressed and ED free initially, with some SD content in the source region. Displacement boundary conditions corresponding to a simple shear strain of 0.1% are imposed. With the onset of plasticity in the source region, excess edge dislocations (α_{13}) of opposite signs generated at the subgrid scale of resolution cancel each other, resulting in zero ED density inside the source region, though a change in the magnitude of L^p_{12} values corresponding to these cancelled dislocations is observed. Since $\boldsymbol{L}^p$ is zero in nonslipped regions, a gradient in L^p_{12} develops at the interfaces of the slipped and nonslipped regions which in turn leads to the generation of α_{13} through (7), as shown in Figure 2c. The α_{13} density generated contributes to flow in the grid elements not containing sources.

Now we discuss size effects at initial yield in cells having a predefined distribution of dislocation sources. Two cubical samples with edge lengths of 0.6 μm and 3.0 μm are considered. The spatial distribution of dislocation sources is shown in Figure 3. Both cells are discretized into a finite element grid with equal element size and are equal to the size of a dislocation source region, in order to avoid any size effect due to the scale of resolution. Displacement boundary conditions corresponding to an engineering simple shearing strain of 0.3% are imposed on the cells as in (16). First, experiments were performed in the context of conventional plasticity theory. Conventional plasticity may be recovered from PMFDM by setting $\boldsymbol{\alpha} = \boldsymbol{0}$ for all times and replacing (2) with

$$\boldsymbol{U}^e = \operatorname{grad} \boldsymbol{u} - \boldsymbol{U}^p, \qquad \dot{\boldsymbol{U}}^p = \boldsymbol{L}^p. \tag{17}$$

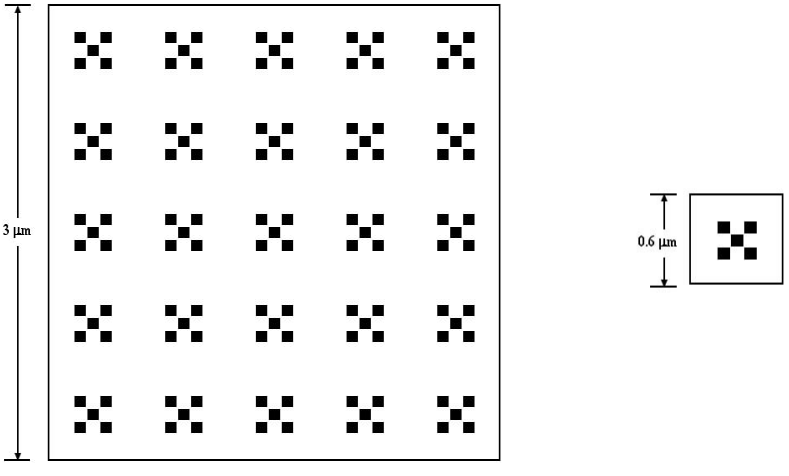

Figure 3. Schematic layout of position of sources (black spots represents the dislocation sources).

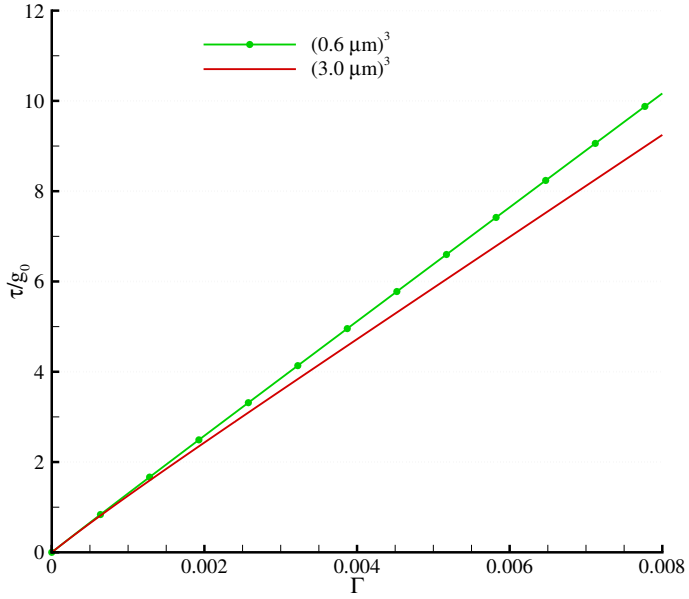

Figure 4. Size effect in simple shear with a predefined spatial distribution of dislocation sources, within a conventional plasticity framework.

Since $\boldsymbol{\alpha} = \mathbf{0}$ in the conventional plasticity framework, nonsource regions are elastic in nature. A size effect is observed for this case as shown in Figure 4, with smaller being harder. It can be inferred from dimensional analysis that in the case of a homogeneous material, there is no length scale in the classical plasticity theory and hence it is not possible to predict size effects in this framework. However, a length scale emerges when a body consisting of discrete dislocation sources is considered. Dimensional analysis of $\boldsymbol{\tau}$ yields

$$\tau = \mu \Phi\left(\frac{\theta_0}{\mu}, \frac{g_s}{\mu}, \frac{g_0}{\mu}, \frac{\dot{\Gamma}}{\dot{\gamma}_0}, m, \Gamma, \frac{s}{H}\right), \tag{18}$$

where H denotes the dimension of the body, s is a representative measure of the distance between the sources (strictly speaking, the size of the sources should also enter as another length-scale parameter), and Φ is a dimensionless function of the arguments shown. It can be deduced from the relation above that if s is kept the same and H is changed, a difference in average response is expected. Thus, it is the spatial layout of dislocation sources that introduces a physical length scale in classical plasticity theory which is otherwise absent. However, the magnitude of that size effect on an average response utilizing discrete sources in an otherwise conventional elastoplastic material falls short of what is qualitatively observed in experiment, indicating the existence of other scale effects and the need for better theory. Nonetheless, this same phenomenology of dislocation sources carries in PMFDM, but now with a greater effect because of the generation of ED at all spatial discontinuities of flow (such as source and nonsource grid elements) and its transport, as well as its accurate accounting in stress response via (1)–(5).

The same numerical experiment is now performed with PMFDM. Accordingly, two cubical cells having edge lengths of 0.6 μm and 3.0 μm and a spatial distribution of dislocation sources as shown in Figure 3, are considered. The area density of sources is identical (0.1) in both cells. The displacement boundary conditions corresponding to a simple shear strain of 0.8% are applied through (16). The

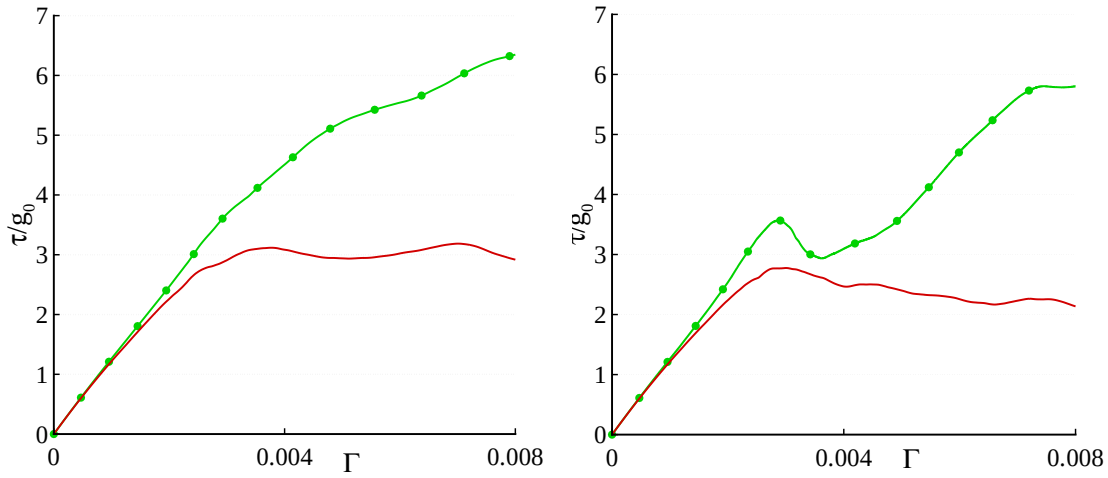

Figure 5. Size effect in simple shear with a predefined source pattern, with hardening rate based on Equation (13) (left) and on Equation (20) (right). The green curves with knots correspond to the 0.6 μm cubes, and the smooth brown curves to the 3.0 μm cubes.

nonsource regions can behave in a plastic manner when ED content is transported through them; however, there is no SD slip rate in these regions.

The average shear stress-strain response, graphed on the left in Figure 5, shows that initial yield strength strongly depends on the cell size with smaller being harder. The size effect is maintained throughout the process of deformation in qualitative agreement with experimentally observed trends [Dimiduk et al. 2005; Greer et al. 2005]. A significant stress drop corresponding to the dislocation activity developing bursts of plastic strain rate is observed in our results which is absent in the experimental results of [Uchic et al. 2004] but may be present in the results from [Greer et al. 2005]. This is due to the fact that numerical experiments performed here correspond to displacement control (similar to those by Greer et al. [2005]) whereas the experimental results presented in [Uchic et al. 2004; Dimiduk et al. 2005] involved mixed (load and displacement) control. The applied load was not allowed to decrease during the experiments performed by Uchic et al. [2004] and Dimiduk et al. [2005] and thus, stress drops are not observed in those studies. The other serrations observed in the experimental results can be obtained in this setup by incorporating a stochastic constitutive response for the plastic strain rate and the ED velocity. We have intentionally stayed away from doing so to demonstrate size effects with the least constitutive input.

In order to understand the cause of size effects in the current framework, dimensional analysis of the applied, (reaction) nominal stress $\boldsymbol{\tau}$ is performed which implies the relation

$$\tau = \mu\Phi\left(\frac{\theta_0}{\mu}, \frac{g_s}{\mu}, \frac{g_0}{\mu}, \frac{\dot{\Gamma}}{\dot{\gamma}_0}, \frac{b}{H}, \alpha_0 H, m, \Gamma, k_0, \eta, \frac{s}{H}\right), \tag{19}$$

where α_0 is a representative measure of the magnitude of the initial ED density field, s is a representative measure of the distance between sources, and Φ is a dimensionless function of the arguments shown. The dimensionless arguments b/H, $\alpha_0 H$, s/H introduce a dependence of average response on the Burgers vector of the material, the geometric proportion of the body, the initial ED density, and the layout of

sources. In these series of tests, the response is independent of $\alpha_0 H$ as the specimens were initially ED-free. Due to the change in spatial distribution of dislocation sources (with associated changes in ED generation), internal stresses may change. Thus, s/H corresponds to the effect of internal stresses of dislocation distributions on average response. The argument (b/H) corresponds to the size effects due to dislocation mobility (12) and strain hardening (13). To evaluate the dependence of the response on internal length scale in strain hardening, the following equation is used for strength rate instead of (13):

$$\dot{g} = \theta_0 \Big(\frac{g_s - g}{g_s - g_0} \Big) \{ |\boldsymbol{\alpha} \times \boldsymbol{V}| + \dot{\gamma} \}. \tag{20}$$

Use of such an equation removes all excess hardening by the ED evolution and interactions as can be seen from the following expression:

$$h = \frac{dg}{dP} = \theta_0 \Big(\frac{g_s - g}{g_s - g_0} \Big), \qquad P = \int \{ |\boldsymbol{\alpha} \times \boldsymbol{V}| + \dot{\gamma} \} dt. \tag{21}$$

Nonetheless, significant size effects are observed as shown in Figure 5, right. Thus, from these sets of computational experiments it may be inferred that a strong size effect at initial yield in PMFDM is primarily due to length scales induced by a discrete SD source distribution and the ED mobility, but not due to strain hardening in the mean-field or stage II sense. This finding is qualitatively consistent with the recent reports by Norfleet et al. [2008] and Rao et al. [2008], both of which show a potent size effect in microcrystal deformation that is associated with the instantaneous mobile dislocation density relative to the imposed loading conditions. Further, the result does not preclude other hardening phenomena, such as the absence of sources as suggested by Greer et al. [2005], or the hardening of sources as suggested by Parthasarathy et al. [2006], from providing alternate or additional hardening mechanisms, respectively. Those effects, while not investigated in the present study, may be represented via alternative selections of the constitutive assumptions of (11)–(13).

Effect of dynamic instability. To study the possibility of dynamical sensitivity of the stress-strain response at initial yield, additional numerical experiments were performed, each corresponding to a small perturbation of the order of machine precision in the boundary condition for displacement. The spatial distribution of sources is assumed to be similar to that used in Section 3.1. It is observed that this small magnitude of perturbation in boundary condition results in a significant difference in the stress-strain response as shown in the top row of Figure 6. There is about 34% variation in the shear stress at 0.8% applied strain for the cell having an edge length of 0.6 μm and 16% for the cell having an edge length of 3.0 μm. The mean shear stress-strain response for each cell size is shown in Figure 6, bottom. The mean values show a cell-size dependence with smaller being harder.

The mechanical response at the macroscopic scale is insensitive to minor perturbations. At the macroscopic scale, sources are considered to be present everywhere in the body. Motivated by this fact, numerical experiments were performed with sources present everywhere in the body, that is, $\boldsymbol{L}^p$ is set active in the entire cell. The four simple shear experiments with varying boundary condition perturbations were performed on the small and big cells. It was observed that in the case of plastically unconstrained cells the stress-strain response up to 0.8% simple shear strain is insensitive to such perturbation in the boundary conditions.

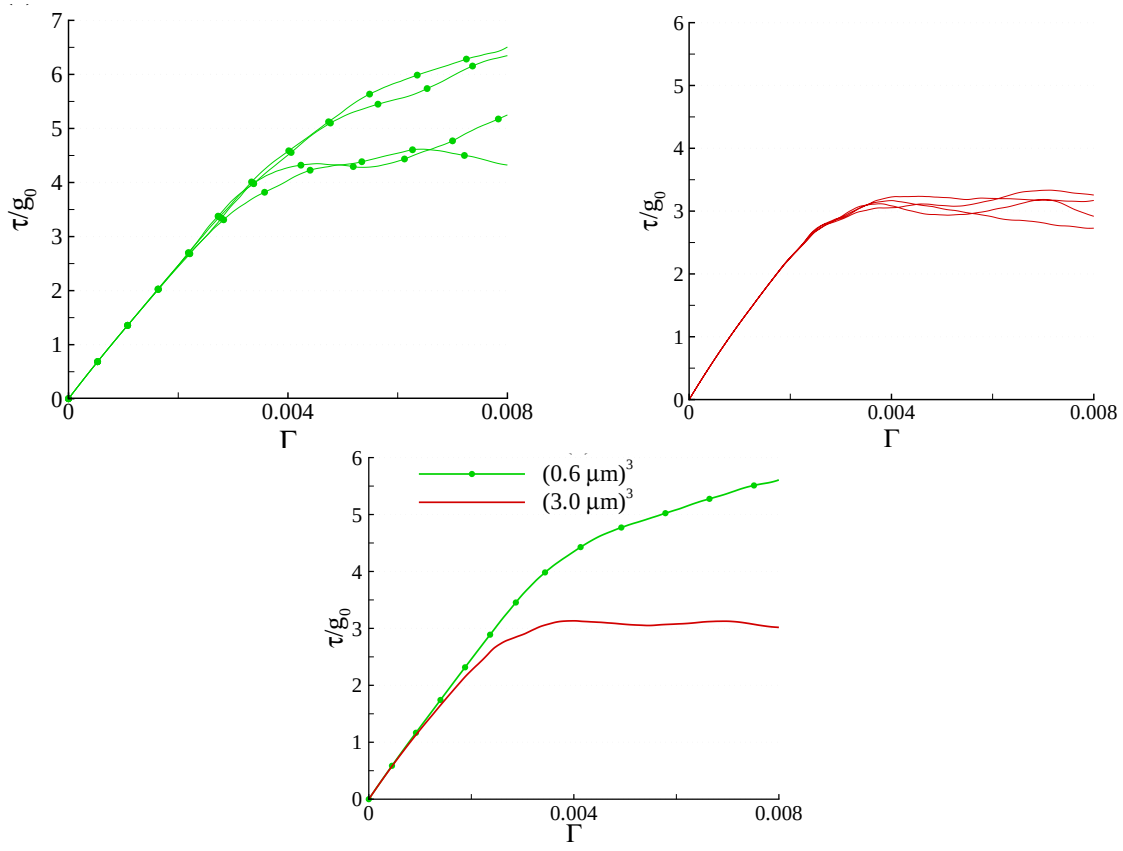

Figure 6. Variability in stress-strain response in simple shear with perturbation in boundary conditions. Top left: 0.6 μm, Top right: 3.0 μm, Bottom: mean response for each of the two sizes.

From these experiments and results presented in [Roy and Acharya 2006] pertaining to the effect of size on stability of stress-strain response in PMFDM, one may infer that discreteness in source distribution and decreasing cell size lead to dynamical sensitivity to perturbations in this model. Note that a qualitatively similar sensitivity to perturbations was found in DD simulations by Deshpande et al. [2001]. Interestingly, there are experimental observations of drastically different responses in samples of the same size when subjected to a prescribed deformation [Uchic et al. 2004]. However, it is not yet possible to deduce from those experiments the degree to which such variation results from differences in initial dislocation configurations and how much may result from small perturbations in the testing. The existence of such intrinsic instability in flow response also emphasizes the importance of the stochastic nature of the material response and the need to average over large numbers of samples to glean the typical material behavior at small scales.

Variation of microstructure. It was deduced from dimensional analysis performed in Section 3.1 that the stress-strain response of PMFDM material depends upon the dimensionless argument s/H. Here we investigate the effect of changes in the spatial distribution of sources in a cell of fixed size containing a fixed source density. Calculations for a cubic cell having an edge length of 3 μm were performed with

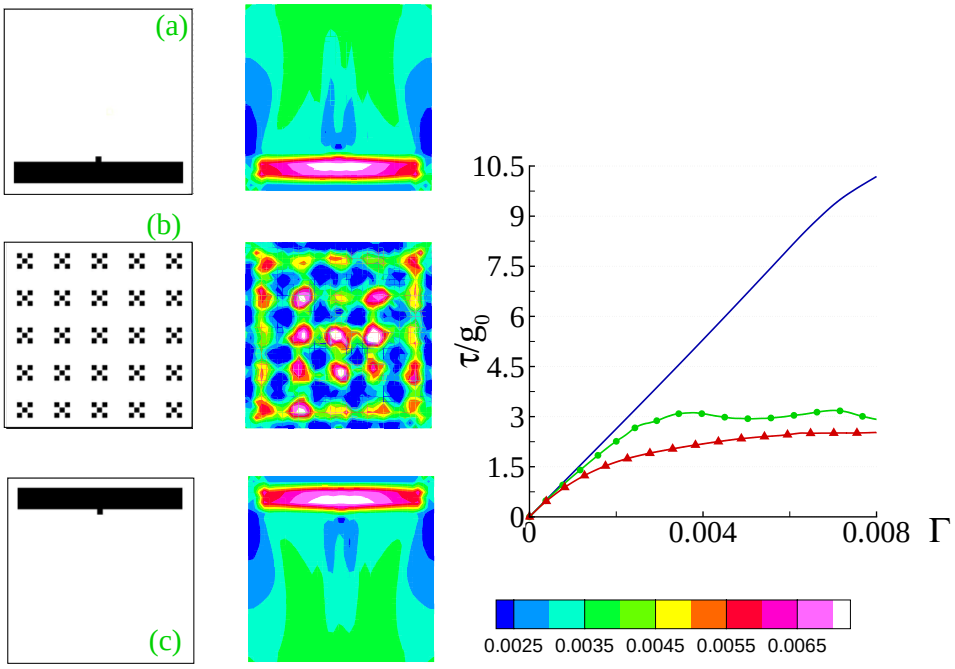

Figure 7. Variability in stress-strain response with change in the source pattern.

three patterns of source distribution, as shown in Figure 7. No perturbations were imposed in this case. The figure shows that average stress at 0.8% applied strain varies approximately from 43 MPa to 180 MPa with varying source pattern. This demonstrates the variation of mechanical response of same-sized cells with a change in microstructure.

Since cells (a) and (c) in Figure 7 are geometrically equivalent (by a 180 degree rotation about the x_3 direction, so the top face of (a) corresponds to the bottom face of (c)), the intuitive expectation is to get the same response in these cases. Reaction forces, however, are measured at the top faces of all cells. The cause for this difference in the reaction force for the two different source patterns is due to the presence of nonzero tractions in the x_1-direction on the left and right faces of the cube due to the imposed displacement boundary conditions for simple shear. Accordingly, the reaction forces on the top need not be equal in magnitude to the reaction forces at the bottom of the cell. The horizontal reaction force on the top face of (a) was indeed identical to the horizontal reaction at the bottom face of (c) as required by symmetry, and likewise for the bottom face of (a) and the top face of (c). The top and bottom face reactions would have to be equal in magnitude from statics for both (a) and (c) if the side faces of the cube were traction free in the 1-direction; this was verified in our numerical experiments.

3.2. ***Size effects due to initial ED distribution.*** Low energy dislocation microstructures are observed in materials. Such structures frequently consist of an array of like-signed dislocations having a low energy arrangement, such as a tilt or twist boundary. Here we investigate the variation of initial yield strength in cells having a predefined spatial distribution of initial ED density of a common sign. Two cubical cells having edge lengths of 0.6 μm and 3 μm are considered. The spatial distribution of initial ED density is shown in Figure 3 for an excess edge-dislocation density of $\alpha_{23} = -2.025 \times 10^{-3}\ \mu\text{m}^{-1}$ prescribed on

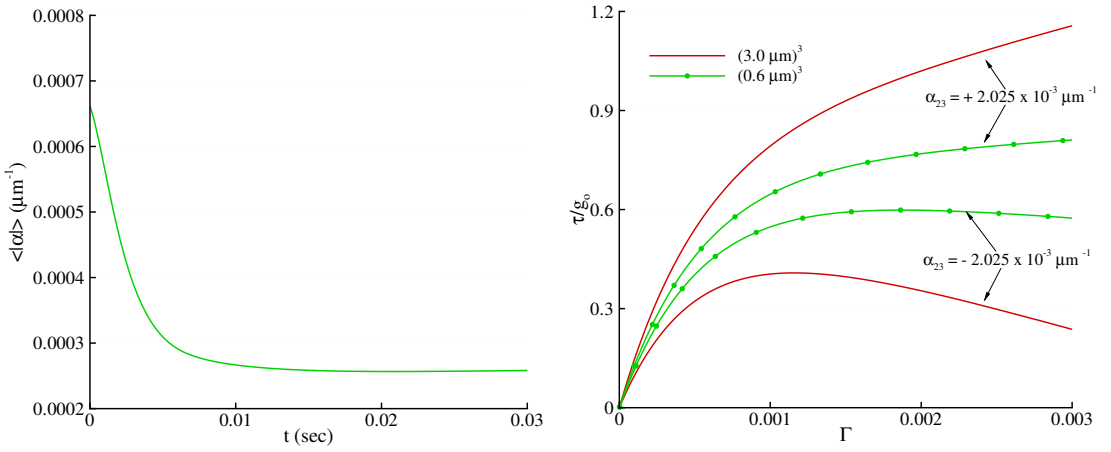

Figure 8. Left: variation in average of $|\boldsymbol{\alpha}|$ over the whole domain with time. Right: size effect in simple shear with a nonzero initial excess dislocation density.

the nodes of shaded elements. In order to obtain an equilibrium state of initial ED density distribution, cells are relaxed in time without any external load. The volume average of $|\boldsymbol{\alpha}|$ is used as a measure of ED content in the cell. Equilibrium is considered to be attained at $t = 0.03$ sec when this measure attains a constant value with respect to time, as shown in Figure 8, left. The strength of the material is assumed to be constant throughout the deformation process, that is, $\dot{g} = 0$ in (13). Once equilibrium is attained, simple shear boundary conditions corresponding to a strain of 0.3% are imposed on the cells. The average shear stress at 0.3% strain for the cell having an edge length of 0.6 μm is 2.5 times higher than that of cell having a 3 μm edge length, as shown in Figure 8, right. Next, a similar test was performed with an initially-prescribed ED density of the same magnitude and opposite in sign. A reversed size effect is observed in this test wherein the larger cell shows a harder response (see again Figure 8b). One can infer from the dimensional analysis performed in (19), that the average response of the material depends upon $\boldsymbol{\alpha}_0 H$ for these cases. With a prescribed $\boldsymbol{\alpha}_0$ among different sized cells a size effect is expected but it is not possible to predict the sense of size effect based on dimensional analysis alone. Due to the complexity and difference in initial ED distribution in these examples, a simpler problem is studied to understand the variation in the sense of size effect depending on the sign of initial ED density. For this simpler case, an initial excess edge-dislocation density $\alpha_{23} = 2.025 \times 10^{-3}\ \mu\text{m}^{-1}$ is prescribed at the center of two cubic cells having edge lengths of 0.6 μm and 3 μm, as shown in Figure 9. The cells are relaxed in time to obtain corresponding equilibrated ED arrangements. Then, displacement boundary conditions corresponding to an engineering simple shearing strain of 0.3% are imposed on the cell. The average shear stress-strain response demonstrates that the smaller cell is indeed harder than the large one. However, a reversed size effect is observed with a change in sign of initial excess dislocation density (see Figure 9). This phenomenon is explained as follows.

Consider a traction free finite cubical block containing a dislocation. In order to understand the resulting stress distribution in the block, we first note that the equations for determining the stress field of a specified ED field in PMFDM are linear; thus supersposition applies. Consider now the stress field of a dislocation in an infinite medium, situated as in Figure 9. This infinite medium stress field

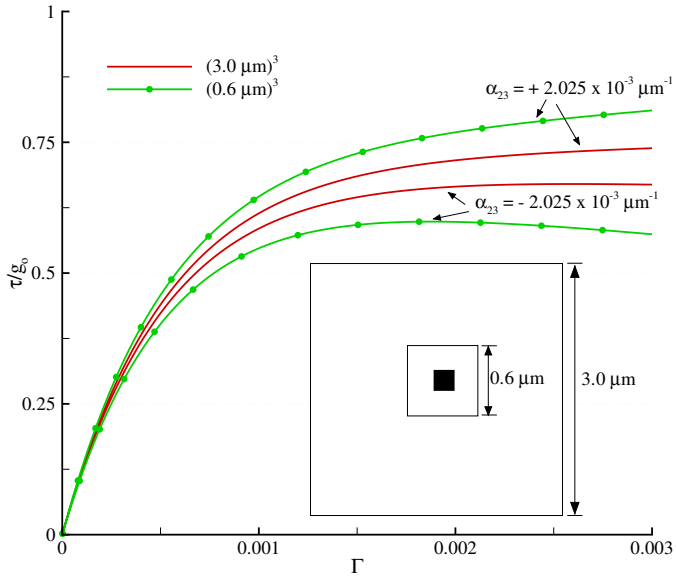

Figure 9. Size effect in simple shear with a nonzero initial excess dislocation density and the new pattern as shown in the inset.

naturally induces tractions on the surface of the finite crystal. Thus, image tractions equal in magnitude and opposite in sign of those induced by the dislocation need to be present on the external surface of the block to satisfy the traction free boundary conditions. Therefore, the *initial stress* field of a traction free finite crystal in equilibrium can be considered as a superposition of the internal stress due to initial ED distribution in the linear elastic infinite medium and the image stress required to satisfy the traction-free boundary conditions. When an external stress is applied, the stress at any point in the finite body is a sum of the initial stress and the applied stress due to boundary conditions (again using superposition) at that point. In the regions having an initially prescribed ED density, less applied stress is required to cause flow if both the initial stress and the applied stress are of the same sign as compared to the case when both are of opposite sign. Now, consider two cubic blocks of different sizes and same initial ED distribution. The magnitude of image stress corresponding to the $(1/r)$ fundamental stress field of a dislocation is higher for the smaller block than the larger block. Accordingly, in the case of the external applied stress being the same sign as the initial stress in the dislocation core region, the smaller cell yields before the large cell (for a constant yield stress). If the sign of the initial ED density is now changed with the direction of applied stressing remaining the same, the initial stress changes sign, the larger cell has a smaller-in-magnitude initial stress that *subtracts* from the applied stress and consequently yields later than the smaller cell.

4. Conclusions

A finite element implementation of PMFDM has been shown to predict size effects at initial yield in plasticity of micron-scale simulation cells. The results are qualitatively consistent with experimental observation in [Uchic et al. 2004; Dimiduk et al. 2005; Greer et al. 2005], as well as with recent discrete dislocation simulations of Weygand et al. [2007], Senger et al. [2008], Tang et al. [2007; 2008], and Rao

et al. [2008]. In the PMFDM framework, size effects are caused by the internal stress of the dislocation distribution, its coupling to the imposed deformation conditions including deformation rate, and natural length scales that enter the theory through strain hardening and the ED velocity. However, an important observation from the computational experiments presented in this paper is that length scales associated with the internal stress due to discrete source patterns and those associated with the plastic strain rate of ED, are solely sufficient for size effects at initial yield within this model. We observe a sensitivity of the overall mechanical response to the presence of discrete source volumes or regions. Size-effect reversals under appropriate circumstances are also observed and explained. For the most part, such sample-scale kinematical size effects have not been treated in discrete dislocation (DD) simulations (notable exceptions being those following the Needleman–Van der Giessen formulation of discrete DD), and have only been peripherally considered in explanations of the widening set of size-effect experiments.

Acknowledgments

We thank Armand Beaudoin for discussions on dynamical sensitivity. Support for this work from the National Science Foundation (Grant number: DMI-0423304), the Dowd-ICES Fellowship at CMU to Saurabh Puri, and the Metallic Materials Division of the AFRL at WPAFB is gratefully acknowledged.

References

[Acharya 2001] A. Acharya, "A model of crystal plasticity based on the theory of continuously distributed dislocations", *J. Mech. Phys. Solids* **49** (2001), 761–785.

[Acharya 2003] A. Acharya, "Driving forces and boundary conditions in continuum dislocation mechanics", *Proc. Royal Soc. A* **459** (2003), 1343–1363.

[Acharya 2004] A. Acharya, "Constitutive analysis of finite deformation field dislocation mechanics", *J. Mech. Phys. Solids* **52** (2004), 301–316.

[Acharya and Beaudoin 2000] A. Acharya and A. J. Beaudoin, "Grain size effect in viscoplastic polycrystals at moderate strains", *J. Mech. Phys. Solids* **48** (2000), 2213–2230.

[Acharya and Roy 2006] A. Acharya and A. Roy, "Size effects and idealized dislocation microstructure at small scales: predictions of a phenonmenological model of mesoscopic field dislocation mechanics: Part I", *J. Mech. Phys. Solids* **54** (2006), 1687–1710.

[Balint et al. 2006] D. S. Balint, V. S. Deshpande, N. A., and E. Van der Giessen, "Size effects in uniaxial deformation of single and polycrystals: a discrete dislocation plasticity analysis", *Modelling Simulation Mater. Sci. Eng.* **14** (2006), 409–422.

[Beaudoin et al. 2000] A. J. Beaudoin, A. Acharya, S. R. Chen, D. A. Korzekwa, and M. G. Stout, "Consideration of grain-size effect and kinetics in the plastic deformation of metal polycrystals", *Acta Metallurgica* **48** (2000), 3409–3423.

[Benzerga and Shaver 2006] A. A. Benzerga and N. F. Shaver, "Scale dependence of mechanical properties of single crystals under uniform deformation", *Scripta Mater.* **54** (2006), 1937–1941.

[Benzerga et al. 2005] A. A. Benzerga, Y. Brechet, A. Needleman, and E. Van der Giessen, "The stored energy of cold work: Predictions from discrete dislocation plasticity", *Acta Materialia* **53** (2005), 4765–4779.

[Deshpande et al. 2001] V. S. Deshpande, A. Needleman, and E. Van der Giessen, "Dislocation dynamics is chaotic", *Scripta Mater.* **45** (2001), 1047–1053.

[Deshpande et al. 2005] V. S. Deshpande, A. Needleman, and E. Van der Giessen, "Plasticity Size effects in tension and compression of single crystals", *J. Mech. Phys. Solids* **53** (2005), 2661–2691.

[Dimiduk et al. 2005] D. Dimiduk, M., M. D. Uchic, and T. A. Parthasarathy, "Size-affected single-slip behavior of pure nickel microcrystals", *Acta Materialia* **53** (2005), 4065–4077.

[Fleck et al. 1994] N. A. Fleck, G. M. Muller, M. F. Ashby, and J. W. Hutchinson, "Strain gradient plasticity: theory and experiment", *Acta Metallurgica et Materialia* **42** (1994), 475–487.

[Frick et al. 2008] C. P. Frick, B. G. Clark, S. Orso, A. S. Schneider, and E. Arzt, "Size effect on strength and strain hardening of small-scale [1 1 1] nickel compression pillars", *Mater. Sci. Eng. A* **489** (2008), 319–329.

[Greer et al. 2005] J. R. Greer, W. C. Oliver, and W. D. Nix, "Size dependence of mechanical properties of gold at the micron scale in the absence of strain gradients", *Acta Materialia* **53** (2005), 1821–1830.

[Ma and Clarke 1995] Q. Ma and D. R. Clarke, "Size-dependent hardness of silver single-crystals", *J. Mater. Res.* **10**:4 (1995), 853–863.

[Norfleet et al. 2008] D. M. Norfleet, D. M. Dimiduk, S. J. Polasik, M. D. Uchic, and M. J. Mills, "Examination of dislocation structures and their relationship to strength of pure nickel microcrystals", *Acta Materialia* **56** (2008), 2988–3001.

[Nye 1953] J. F. Nye, "Some geometrical relations in dislocated crystals", *Acta Metallurgica* **1** (1953), 153–162.

[Parthasarathy et al. 2006] T. A. Parthasarathy, S. I. Rao, D. M. Dimiduk, M. D. Uchic, and D. R. Trinkle, "Contribution to size effect of yield strength from the stochastics of dislocation source lengths in finite samples", *Scripta Mater.* **56** (2006), 313–316.

[Rao et al. 2008] S. I. Rao, D. M. Dimiduk, T. A. Parthasarathy, M. D. Uchic, M. Tang, and C. Woodward, "Athermal mechanisms of size-dependent crystal flow gleaned from three dimensional discrete dislocation simulations", *Acta Materialia* **56** (2008), 3245–3259.

[Roy and Acharya 2006] A. Roy and A. Acharya, "Size effects and idealized dislocation microstructure at small scales: predictions of a phenonmenological model of mesoscopic field dislocation mechanics: Part II", *J. Mech. Phys. Solids* **54** (2006), 1711–1743.

[Senger et al. 2008] J. Senger, D. Weygand, P. Gumbsch, and O. Kraft, "Discrete dislocation simulations of the plasticity of micro-pillars under uniaxial loading", *Scripta Mater.* **58** (2008), 587–590.

[Stölken and Evans 1998] J. S. Stölken and A. G. Evans, "A microbend test method for measuring the plasticity length scale", *Acta Materialia* **46**:14 (1998), 5109–5115.

[Tang et al. 2007] H. Tang, K. W. Schwarz, and H. D. Espinosa, "Dislocation escape-related size effects in single-crystal micropillars under uniaxial compression", *Acta Materialia* **55** (2007), 1607–1616.

[Tang et al. 2008] H. Tang, K. W. Schwarz, and H. D. Espinosa, "Dislocation-source shutdown and the plastic behavior of single-crystal micropillars", *Phys. Rev. Letters* **100** (2008), 185503–1–4.

[Uchic et al. 2004] M. D. Uchic, D. M. Dimiduk, J. N. Florando, and W. D. Nix, "Sample dimensions influence strength and crystal plasticity", *Science* **305** (2004), 986–989.

[Varadhan et al. 2006] S. N. Varadhan, A. J. Beaudoin, A. A., and C. Fressengeas, "Dislocation transport using an explicit Galerkin/least-squares formulation", *Modelling Simulation Mater. Sci. Eng.* **14** (2006), 1245–1270.

[Weygand et al. 2007] D. Weygand, M. Poignant, P. Gumbsch, and O. Kraft, "Three-dimensional dislocation dynamics simulation of the influence of sample size on the stress–strain behavior of fcc single-crystalline pillars", *Mater. Sci. Eng. A* (2007). in press.

Received 16 Jul 2008. Revised 14 Mar 2009. Accepted 4 Jun 2009.

SAURABH PURI: saurabhp@caltech.edu
Department of Mechanical Engineering, California Institute of Technology, Pasadena, CA 91125, United States

ANISH ROY: A.Roy3@lboro.ac.uk
Wolfson School of Mechanical and Manufacturing Engineering, Loughborough University, Leicestershire, LE11 3TU, United Kingdom

AMIT ACHARYA: acharyaamit@cmu.edu
Department of Civil and Environmental Engineering, Carnegie Mellon University, Pittsburgh, PA 15213, United States

DENNIS DIMIDUK: dennis.dimiduk@wpafb.af.mil
Air Force Research Laboratory, Materials and Manufacturing Directorate, AFRL/MLLM Bldg. 655, 2230 Tenth Street, Wright-Patterson AFB, OH 45433-7817, United States